

Chapter 2

Control Issues in Solar Systems

2.1 Introduction

This chapter is devoted to introduce the main issues involved in the control of solar energy systems. Four different levels can be distinguished: (i) the control of the solar collector units, (ii) solar radiation estimation and forecast, (iii) the control of the energy conversion systems and (iv) the overall control of the complete process.

The control of the solar collecting systems consist of controlling the solar collectors movements in such a way that the maximum solar energy is collected at any time. In the case of dish collectors with two degrees of freedom, the controls system keeps the collector surface perpendicular to the solar vector. In the case of solar trough or collectors with one degree of freedom, the mission of the controller is to maintain the solar collector surface normal as close as possible to the Sun vector. The controller has to compute the Sun vector, which depends of the geographical position of the collector and the date and time of day. The position of the collectors is then determined with a trigonometrical computation and this is sent to the servo controlling the collector axes. Fine tracking is obtained in some cases by using signals which depend on the angle formed by the collector surface normal and the solar vector.

In the case of solar power towers or Fresnel linear solar collectors, the reflecting mirrors have to be moved in such a way that the solar radiation is reflected on the central receiver or the receiver tube. The heliostats have to be controlled in such a way that the solar radiation is reflected on the central receiver. The heliostat surface normal should be in the bisectrix of the angle formed by the solar vector and the vector joining the center of the heliostat reflecting surface and the central receiver.

In order to control solar energy system, it is very important both to know the actual values of solar irradiance and even to be able to forecast this variable within different time windows to be used for control and operation planning purposes. Thus, adequate sensors to obtain values for solar irradiance are used in these kinds of plant (mainly pyranometers and pyrhelimeters) and different algorithms to provide estimations of future values of solar irradiance where the solar plant is located.

The control of the variables associated to the solar conversion units depends very much on the type of system. In the case of photovoltaic (PV) systems, this involves

the control of the voltage and intensity produced by the solar cells in order to operate at the maximum efficiency point and the controls of the associated DC/AC conversion power electronics. In the case of thermal solar plants, the solar energy heats up a fluid which is then used to produce steam necessary to drive the turbines. The variables to be controlled at this level are the temperatures and flows of the heat collecting fluid. The main difference with other power plants is that the main source of energy, the solar radiation, cannot be manipulated. An important part of this book is dedicated to this issue. The heated HTF is then used to produce steam and from this point, the controls at this level do not differ much from the control of other thermal plants.

The upper control level takes care of the operation of the complete solar system. The control decides what amount of energy is produced and delivered and what amount is stored and which are the set points of the main process variables at any given moment. Since the solar radiation varies along the day, the plant is rarely at a steady state condition and the determination of the optimal operating points should be done dynamically. Solar energy is intermittent and is not available when needed and where needed, and because of this the integration of solar energy plants in the electrical grid is a challenging problem. An efficient operation of solar plants with energy storage systems could allow a closer match between solar plants power generation and electrical power demand. Furthermore, proposals of new price mechanisms are appearing continuously with the liberalization of the energy prices and they are considered to be a fundamental part of the Smart Grid concept. The price fluctuations tend to correlate well with the demand and an efficient operation of a solar power plant installation requires all of these aspects to be considered.

2.2 Sun Tracking

2.2.1 *The Need for Tracking the Sun*

In order to collect solar energy on the Earth, it is important to know the angle between the Sun's rays and a collector surface (aperture). The collector aperture is defined as the surface of the plane normal to the Sun rays through which non-concentrated radiation enters the collector where it is reflected. The aperture angle in parabolic trough collectors (PTC) is the angle between the axis of the parabola and the line connecting the focus with one end of that parabola.

When a collector (its aperture normal) is not pointing directly at the Sun, some of the energy that could be collected is being lost [359].

In Sect. 1.2.5 the Sun's position angles relative to Earth-center coordinates (ϕ , δ_s , and ω_s) were defined. In the design of solar energy systems it is important to be able to predict the angle between the Sun's rays and a vector normal (perpendicular) to the aperture of the collector. This angle is called the angle of incidence θ_i . The tracking angle ρ_t is the amount of rotation that collectors require to place their aperture normal to the Sun's central ray.

A characteristic fundamental to the capture of solar energy is that the amount of energy incident on a collector is reduced by a fraction equal to the cosine of the angle between the collector surface and the Sun's rays. Knowing the position of the collector and the position of the Sun, equations may be used to predict the fraction of incoming solar energy that falls on the collector [359].

Concentrating solar technologies can make use of only direct solar irradiance, that is, the beam that come directly from the solar disk and not those that could be reflected from the surroundings. Therefore, solar collectors must be equipped with systems that enable the collecting surface to maintain the orientation necessary to reflect and concentrate the beam on the receiver. The Sun's position in the sky vault varies slowly during the day, in a trajectory above the horizon. Such a trajectory is different every day of the year.

2.2.1.1 The Solar Incidence Angle

Each of the CSP systems considered here tracks the Sun in a different way. As described in Chap. 1, the Sun's position with respect to the observer can be described by two angles, the azimuth angle and the elevation angle. A third angle is crucial to calculate the effective solar power usable by a solar collector; this is the incidence angle (θ_i). The effective collecting area is reduced by the cosine of the angle formed by the normal to the collecting surface and the Sun position vector at any instant. The incident solar power must be reduced by applying the factor $\cos(\theta_i)$ in the calculations. This is clearly a reducing factor as $-1 \leq \cos(\theta_i) \leq 1$. Most of the systems considered in this book are tracking the Sun, but most of them do not face it directly, so this *imperfect* tracking leads to the effect of the *cosine factor*. Then, the way to calculate the incident power on the receiver is

$$P_{sol} = E_b G \cos(\theta_i) \quad (2.1)$$

where E_b is the direct normal irradiance [W/m^2], G is the collector aperture area [m^2] and $\cos(\theta_i)$ is the cosine of the incidence angle.

2.2.1.2 The Cosine Factor Effect in the Different Solar-Tracking Systems

A PTC tracks the Sun on azimuth or elevation. The collector can be oriented East–West and track the Sun on elevation, or vice versa. The reflected beam is incident on a tube placed in the focal line of the collector, which moves along with it. Once the horizontal coordinates of the Sun are known, $\cos(\theta_i)$ can be calculated as follows [184]:

- For a collector with axis oriented East–West:

$$\cos(\theta_i) = (1 - \cos^2(\delta_s) \sin^2(\omega_s))^{\frac{1}{2}} \quad (2.2)$$

- For a collector with axis oriented North–South:

$$\cos(\theta_i) = \left((\sin(\phi) \sin(\delta_s) + \cos(\phi) \cos(\delta_s) \cos(\omega_s))^2 + \cos^2(\delta_s) \sin^2(\omega_s) \right)^{\frac{1}{2}} \quad (2.3)$$

Linear Fresnel collectors are quite similar, except that the receiver, located well above a set of mobile flat mirrors, does not move, so tracking is on one-angle, or single-axis.

In a central receiver system, a heliostat tracks the Sun in such a way that the reflected rays are incident on a single receiver located on top of a tower. Although this tracking is two-axis, the cosine factor also appears, as the normal to the reflecting surface has an angle of deviation with respect to the Sun position vector.

The following formula can be used to calculate the cosine factor for a given heliostat [161]:

$$\cos(\theta_i) = \frac{\mathbf{n}^T \cdot \mathbf{H}}{\|\mathbf{n}\| \cdot \|\mathbf{H}\|} \quad (2.4)$$

$$\begin{aligned} \mathbf{n} &= [\cos(\alpha_n) \sin(a_n), -\cos(\alpha_n) \cos(a_n), \sin(\alpha_n)]^T \\ \mathbf{H} &= [\cos(h_t) \sin(a_t), -\cos(h_t) \cos(a_t), \sin(h_t)]^T \\ \mathbf{S} &= [\cos(h_s) \sin(a_s), -\cos(h_s) \cos(a_s), \sin(h_s)]^T \end{aligned}$$

where h_s and a_s are the solar altitude and azimuth angles, h_t and a_t are the fixed tower vector altitude and azimuth angles shown in Fig. 2.1 and h_n and a_n are the heliostat-normal altitude and azimuth angles, measured in the same way as h_s and a_s .

The most efficient tracking is done by the parabolic dish systems, in which tracking is two-axis and the parabola faces the Sun directly when in tracking mode, so there is no *cosine factor* effect. This is possible because the parabola has a single focal point, where the receiver may be placed.

2.2.2 Tracking Systems

A solar tracker is a device that points a solar collector mechanism toward the Sun or directs a reflector mechanism in such a way that it reflects the maximum energy onto a collector device. The relative position of the Sun in the sky changes both with the seasons and the time of day. As has been mentioned in the previous section, the solar power received by a solar collector is equal to the solar irradiance received at that location multiplied by the device surface and by the cosine of the angle formed by the Sun's rays and the normal surface. There are many types of solar-tracking mechanism with different accuracies. Solar tracking can be implemented by using one-axis and for higher accuracy, two-axis Sun-tracking systems.

Power tower heliostats need a good degree of accuracy to ensure that the power is reflected onto the receiver which can be situated hundreds of meters from the

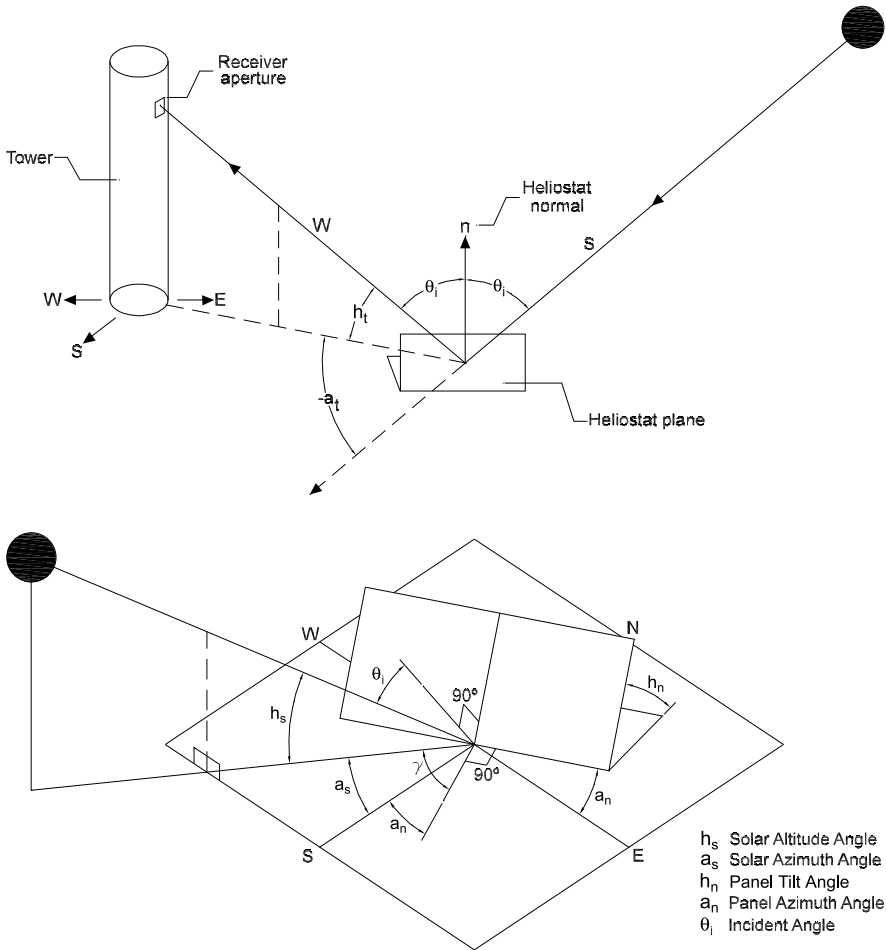


Fig. 2.1 Tracking and incidence angles for a heliostat

heliostat. Little accuracy is required for non-concentrating applications; in fact, most of these applications work without any solar tracking at all.

Tracking can significantly increase the amount of energy produced, especially in the early morning and late afternoon when the cosine of the angle of the direct solar irradiance with the surface normal is smaller.

In [263], a review of principle and Sun-tracking methods is developed focused on PV panels, but useful for other kinds of solar device. All tracking systems have all/some of the following characteristics:

- Single column structure or of parallel console type.
- One or two moving motors.
- Light sensing device.
- Autonomous or auxiliary energy supply.

- Light following or moving according to the calendar.
- Continuous or step-wise movement.
- Tracking all year or all year except winter.
- Orientation adjustment with/without the tilt angle adjustment.

Sun-tracking systems are usually classified into two categories [263]:

- Passive (mechanical) solar trackers are based on thermal expansion of a matter (usually Freon) or on shape memory alloys. Usually this kind of tracker is composed of couple of actuators working against each other which are, by equal illumination, balanced.
- Active (electrical) trackers can be categorized as microprocessor and electro-optical sensor based, computer-based controlled date and time, auxiliary bifacial solar cell based and a combination of these three systems. Electro-optical solar trackers are usually composed of at least one pair of anti-parallel connected photo-resistors or PV solar cells which are, by equal intensity of illumination of both elements, electrically balanced so that there is either no or negligible control signal on a driving motor. In auxiliary bifacial solar cell, the bifacial solar cell senses and drives the system to the desired position and in PC controlled date and time based, a computer calculates the Sun positions with respect to date and time with algorithms and create signals for the system control.

Many fast algorithms for calculating the Sun position used in engineering applications requiring little computation can be found in the literature. The well-known Spencer formula has a maximal error greater than 0.25° . There have been a number of algorithms proposed in literature [56, 102, 163] which increase precision without incurring high computational efforts. These algorithms work correctly for limited periods of time. There are also high-precision astronomical algorithms to compute the Sun's position with an error of less than 0.0003° over a very long period of time (2000 B.C.–6000 A.C.); they require a large amount of computation.

2.3 Solar Irradiance over a PTC

The global solar irradiance E_g over a horizontal surface that does not collect radiation due to reflection or diffusion is composed of the direct solar irradiance E_b (coming directly from the solar disc and measured over a plane normal to the direction of the solar irradiance) and the diffuse irradiance E_d (that subjected to absorption/diffusion processes in the atmosphere and measured over a horizontal plane) according to

$$E_g = E_b \cos(\theta_i) + f_{di} E_d \quad (2.5)$$

where f_{di} is the amount of diffuse irradiance intercepted by the surface. For concentrating collectors [305]:

$$f_{di} = \frac{1}{C_g} \rightarrow E_g = E_b \cos(\theta_i) + \frac{1}{C_g} E_d \quad (2.6)$$

where C_g is the geometrical concentration factor, that is, the ratio between the collector aperture surface and that of the absorbent tube (the part of the solar collector receiving the concentrated solar radiation and transforming it in thermal energy). For PTC with concentration factors over 14, the second term in the right hand of the equation can be neglected, so that $E_g \approx E_b \cos(\theta_i)$.

2.3.1 Optical and Geometrical Losses in a PTC

Optical efficiency η_{opt} is defined as the factor that takes into account energy losses between the reference solar power, P_{sol} , and the power absorbed by the receiver, P_{abs} . These energy losses are optical and geometric and are due to the following:

- Primary concentrator parabolic mirrors are not perfect reflectors, so their specular reflectivity, r , has to be taken into account.
- The glass cover is not perfectly transparent, but lets only part of the incident radiation through, which is determined by its transmissivity, $\tau_{sol,c}$.
- The absorber surface has a certain solar radiation absorptance $\alpha_{sol,A}$.
- There may be errors in the positioning of the receiver on the axis of the parabola which is formed by the mirrors, errors in the parabolic mirror shape itself, errors in solar tracking which cause reflected rays not to intercept the absorber, etc. All of these possible errors are included in the intercept factor, γ_A .

Power absorbed by the receiver, P_{abs} , may therefore be said to be given by

$$P_{abs} = G E_b \cos(\theta_i) r(\theta_i) \tau_{sol,c}(\theta_i, \lambda) \alpha_{sol,A}(\theta_i, \lambda) \gamma_A(\theta_i) \quad (2.7)$$

This equation emphasizes that the variables in it depend on the angle of incidence of the irradiance, θ_i , and for absorptance of the absorber and transmittance of the cover, on wavelength range, λ , which characterizes the incident radiation. Adding $\alpha_{sol,A}(\theta_i)$ and $\tau_{sol,c}(\theta_i)$ to the integrated absorptance of the absorber and transmittance of the cover, respectively, in relation to the solar radiation spectrum, the above expression may be simplified as

$$P_{abs} = G E_b \cos(\theta_i) r(\theta_i) \tau_{sol,c}(\theta_i) \alpha_{sol,A}(\theta_i) \gamma_A(\theta_i) \quad (2.8)$$

According to the definition of optical efficiency, η_{opt} , and according to the nomenclature used above, we have

$$\begin{aligned} \eta_{opt} &= \frac{P_{abs}}{P_{sol}} \\ \rightarrow \quad &\text{if } P_{sol} = G E_b \cos(\theta_i) \\ \rightarrow \quad &\eta_{opt}|_{E_b \cos(\theta_i)} = r(\theta_i) \tau_{sol,c}(\theta_i) \alpha_{sol,A}(\theta_i) \gamma_A(\theta_i) \\ &\text{if } P_{sol} = G E_b \\ \rightarrow \quad &\eta_{opt}|_{E_b} = r(\theta_i) \tau_{sol,c}(\theta_i) \alpha_{sol,A}(\theta_i) \gamma_A(\pi) \cos(\theta_i) = \eta_{opt} \end{aligned} \quad (2.9)$$

The definition of efficiency uses direct irradiance, E_b , as the reference, so the second equation in (2.9) is used. The incidence angle modifier, $\kappa(\theta_i)$, is the factor that takes all of the geometric and optical measurements into account, because the incident irradiance is at a certain angle θ_i , that is,

$$\kappa(\theta_i) = \frac{\eta_{opt}(\theta_i)}{\eta_{opt}(\theta_i = 0^\circ)} = \frac{\eta_{opt}}{\eta_{opt,0^\circ}} \quad (2.10)$$

Optical efficiency that considers normal incident irradiance ($\theta_i = 0^\circ$) is called nominal optical performance, $\eta_{opt,0^\circ}$. Optical performance can thus be expressed as

$$\eta_{opt} = \eta_{opt,0^\circ} \kappa(\theta_i) \quad (2.11)$$

$$\eta_{opt,0^\circ} = r(0^\circ) \tau_{sol,c}(0^\circ) \alpha_{sol,A}(0^\circ) \gamma_A(0^\circ) \quad (2.12)$$

and according to the second equation in (2.9),

$$\kappa(\theta_i) = \frac{r(\theta_i)}{r(0^\circ)} \frac{\tau_{sol,c}(\theta_i)}{\tau_{sol,c}(0^\circ)} \frac{\alpha_{sol,A}(\theta_i)}{\alpha_{sol,A}(0^\circ)} \frac{\gamma_A(\theta_i)}{\gamma_A(0^\circ)} \cos(\theta_i) \quad (2.13)$$

The incidence angle modifier can also be provided as a polynomial expression on the incidence angle θ_i . Some authors, however, prefer to distinguish $\cos(\theta_i)$ in the modifier by the angle of incidence, $\kappa(\theta_i)$, writing Eq. (2.11) as

$$\begin{aligned} \eta_{opt} &= \eta_{opt,0^\circ} \kappa(\theta_i) \cos(\theta_i) \\ \text{considering } \kappa(\theta_i) &= \frac{r(\theta_i)}{r(0^\circ)} \frac{\tau_{sol,c}(\theta_i)}{\tau_{sol,c}(0^\circ)} \frac{\alpha_{sol,A}(\theta_i)}{\alpha_{sol,A}(0^\circ)} \frac{\gamma_A(\theta_i)}{\gamma_A(0^\circ)} \end{aligned} \quad (2.14)$$

One of the geometric losses included by definition in the intercept factor, $\gamma_A(\theta_i)$, is the irradiance at the ends (because the collector has a finite length). Some authors [305] also prefer to distinguish this term in the modifier by the angle of incidence since it is merely a geometric reduction factor. They would therefore write Eq. (2.11) as

$$\eta_{opt} = \eta_{opt,0^\circ} \kappa(\theta_i) \Gamma(\theta_i), \quad \text{where } \Gamma(\theta_i) = 1 + \frac{f_d}{L} \left(1 + \frac{G}{48 f_d^2} \right) \tan(\theta_i) \quad (2.15)$$

where f_d is the focal distance of the parabolic mirrors, G is the aperture width and L is the collector length. In any case, with a constant loss coefficient, the higher the optical efficiency, the higher collector performance is. Thus, the higher the variables that define it, the better the performance of the collectors will be. Mirror reflectivity and transmittance of the cover are largely determined by how clean the collector is. It is therefore important to have suitable collector maintenance and cleaning strategy in a PTC plant.

In this book, the measured direct solar irradiance and the corrected solar irradiance will be denoted I . The value of this variable is obtained directly from a pyrheliometer $I = E_b$ and it is going to be used for feedforward control purposes within a control algorithm $I = E_b \cos(\theta_i) S$, where $S = S_{ref} \eta_{opt}$, S_{ref} being the reflecting surface of the collector field's mirrors. A more detailed description of the model can be found in [38].

2.3.2 Thermal Losses in a PTC

Besides optical and geometric losses, thermal losses are important in PTC and they are occurred mainly in two places: in the absorber tube and in the HTF pipe.

Heat losses associated with the absorber tube are made of: heat loss by conduction through the pipe supports, losses by radiation, convection and conduction from metal tube into the glass cover and losses by convection and radiation from the tube crystal to the environment. In those absorber tubes in which vacuum exists between the metal tube and the glass, convection losses from the metal tube into the glass are eliminated and only losses by radiation and small ones by conduction between the glass-metal joint exist.

Although each of the heat losses could be calculated analytically, in practice a global heat losses coefficient from the absorber tube to the ambient is defined, in such a way that

$$P_{m \rightarrow a} = H_l \pi D_m L (\bar{T}_f - T_a) = H_l \pi D_m L \bar{\Delta T} \quad (2.16)$$

where $\bar{T}_f = \frac{T_{out} + T_{in}}{2}$ is the mean temperature of the HTF (notice that some authors use instead the mean temperature of the metal absorber \bar{T}_m), T_a is the ambient temperature, T_{out} the outlet HTF temperature, T_{in} the inlet HTF temperature, D_m is the outside diameter of the absorber pipe and L is the length of the tube (length of the PTC). In (2.16) the global heat loss coefficient is given by surface unit of the absorber tube [$W/(m^2 K)$]. It can be defined by collector aperture surface unit $H_{lcol} = H_l / C_g$ [$W/(m_{col}^2 K)$]. In both cases, the coefficient can be obtained from experiments within the design temperature range. It can be expressed also in polynomial form as

$$H_l = a + b(\bar{T}_f - T_a) + c(\bar{T}_f - T_a)^2 \quad [W/(m^2 K)]$$

2.3.3 PTC Efficiency

The incident power on a PTC was given in Eq. (2.1). The thermal power given by a PTC can be computed in terms of enthalpy increment that the HTF experiments when flowing through the collector:

$$P_{m \rightarrow f} = \dot{m}(h_{out} - h_{in}) \quad [W] \quad (2.17)$$

where \dot{m} is the mass flow rate [kg/s], h_{in} is the specific enthalpy of the HTF at the collector inlet [J/kg] and h_{out} is the specific enthalpy of the HTF at the collector outlet [J/kg].

Three different efficiencies can be defined in a PTC: global efficiency $\eta_{global} = \eta_{col}$, optical efficiency with an incidence angle of 0° ($\eta_{opt,0^\circ}$) and the thermal efficiency (η_{th}), plus the incidence angle modifier $\kappa(\theta_i)$. The global efficiency considers all the losses (optical, geometrical and thermal) and can be obtained as

$$\eta_{col} = \frac{P_{m \rightarrow f}}{P_{sol}} = \eta_{opt,0^\circ} \kappa(\theta_i) \eta_{th} \quad (2.18)$$

The thermal efficiency η_{th} depends on the working temperature of the metallic absorber tube and can be given as a function of the ambient temperature and the absorber tube temperature for a determined value of the direct solar irradiance.

Considering the reference solar irradiance to be equal to the global irradiance, the efficiency of a PTC is given by

$$\eta|_{E_b \cos(\theta_i)} = \eta_{opt}|_{E_b \cos(\theta_i)} - \frac{H_l}{C_g} \frac{(\bar{T}_f - T_a)}{E_b \cos(\theta_i)} \quad (2.19)$$

Many authors [305] use for tracking PTC as reference solar irradiance the direct solar irradiance; the efficiency is given by

$$\eta|_{E_b} = \eta_{opt}|_{E_b} - \frac{H_l}{C_g} \frac{(\bar{T}_f - T_a)}{E_b} \quad (2.20)$$

2.4 Solar Irradiance Estimation and Forecast

Nowadays, there exist many systems where disturbance estimation would be needed to improve the overall performance of the control system. Some examples can be found in control systems for renewable power generation, especially for solar thermal and photovoltaic energy, where the solar radiation is used as the main energy source. Solar irradiance is a changing variable that can be perturbed by clouds, temporal dust concentration, vapor concentration, etc. Many of these changes have a temporal presence and can vary from one season to another. For this reason, some estimations about the future behavior of the solar radiation is required to optimize the process performance and minimize the use of auxiliary energy sources [288].

As a first approach, solar radiation estimation can be used for the following purposes:

1. Selection of the best location to build the solar plant (maximization of the solar resource).
2. Long-term operation planning, to estimate the power that can be supplied to the electrical network (daily and monthly prediction values [248]). At these higher decision-making levels, weather information is exploited indirectly by mapping it to economic variables such as user power demands [420].
3. Short-term operation planning, grid integration and operational control under FIT regulations (the regional or national electricity utilities have to buy renewable electricity at above-market rates set by the government). The prediction horizon in this case can be considered as short-term for prediction up to several hours. As pointed out in [311], short-term forecasts are needed for operational planning, switching sources, programming backup and short-term power purchases, as well as for planning for reserve usage and peak load matching. Also, actual measurements or estimations of the solar radiation are used to control the fundamental variables.

Table 2.1 Basic characteristics of solar radiation forecasting

Forecasting horizon:	Short-term	Long-term
Purpose (spatial nature):	Local	Global
Kinds of model:	Physics-based models	Statistical models

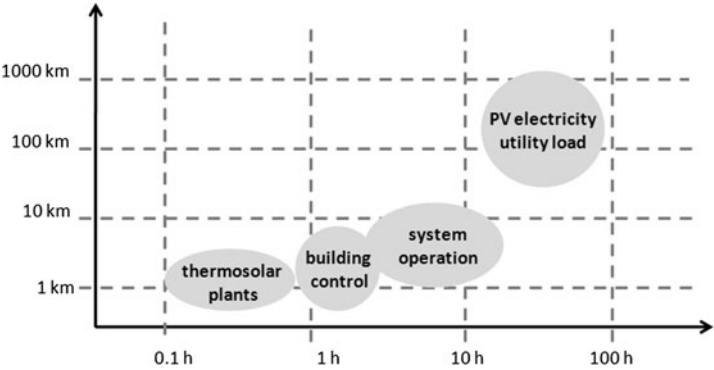


Fig. 2.2 Spatial and temporal scales of target applications, [175]

The previous objectives are also related to the existing methods to estimate solar radiation, which can be characterized by the prediction horizon length, their spatial character and the selected methodology (Table 2.1). Figure 2.2 shows typical target applications for solar radiation forecasting and their respective spatial and temporal scales [175]. Notice that, as pointed out in [420], major weather prediction centers, such as the European Centre for Medium-Range Weather Forecasts (ECMWF) and the US National Centers for Environmental Prediction (NCEP), are capable of producing high-precision weather forecasts several times a day, thanks to improved models of the atmosphere, greater availability of atmospheric data, increased computational power and the continued improvement of state estimation algorithms. Anyway, the models must be reconciled to the most recent observations. This state estimation problem is called in the weather forecast literature the data assimilation problem, where stochastic approaches as those treated in this section are used internally.

In the first case (location optimization), the most common methods to estimate the solar resource are based on the combination of local measurements (climate stations), satellite images and digital elevation models [62, 193, 374], where mainly physics-based models and artificial neural networks (ANN) are used for data fusion. In the second case (operation planning), the main approaches are based on the National Meteorological Institutes forecasts, historical datasets and satellite images to provide long-term solar radiation forecast. In [312] a comparison of different methods for two-days forecast is performed. The methods are based on the National digital forecast database (NDFD) of NOAA (<http://www.weather.gov/ndfd/>), the ECMWF (<http://www.ecmwf.int>) and the Weather research and forecasting (WRF) model (<http://www.wrf-model.org>) with first input of Global Forecast System (GFS)

model. In the third approach (short-term operation planning and control), direct measurements from solar irradiance sensors (mainly pyrheliometers and pyranometers) are used both for feedforward control and short-term solar irradiance forecast, sometimes combined with fish-eye cameras (total sky imagers that take hemispherical sky photographs), ceilometers (recording cloud height) and satellite images [175, 214].

In this book the interest is focused on easy methods to perform a short-term solar irradiance forecast (daily solar radiation estimation). The estimation of solar irradiance on a horizontal surface can be mainly performed based on physical models or data-driven models. As pointed out by [378] and references therein, there exist mainly three methodologies for the estimation of horizontal global solar irradiance:

1. Estimation based on physical processes including complex radiative transfer models. The physical interactions between solar radiation and the terrestrial atmosphere (such as Rayleigh scattering, radiative absorption by ozone and water vapor and aerosol extinction) are considered. These models are also known as parametric models [399].
2. Approaches based on the traditional and long-utilized Ångström's linear approach and its modifications which is based on measurements of sunshine duration [14], providing empirical relationships between the ratio of the global solar radiation on a horizontal surface at the Earth's surface and at the top of the atmosphere and the percent possible sunshine (i.e. observed bright sunshine to maximum possible sunshine hours). These models are also known as decomposition models [399], as they usually use information only on global radiation to predict the beam and sky components.
3. Estimation based on data and statistical models represented by time-series or ANN, which can be based on sunshine duration measurements but also on other climatological parameters.

In [399] and cited references, solar radiation models for predicting the average daily and hourly global irradiance, beam irradiance and diffuse irradiance are reviewed. Examples of estimation based on the first two categories indicated previously are developed to predict the beam component or sky component based on other more readily measured quantities.

In what follows, selected examples of the mentioned models are developed based on the authors' experience.

2.4.1 Physics-Based Models

As pointed out by [399], parametric models require detailed information of atmospheric conditions. Meteorological parameters frequently used as predictors include the type, amount and distribution of clouds or other observations, such as the fractional sunshine, atmospheric turbidity and precipitable water content. Two well-known parametric models used for solar energy applications are:

- The ASHRAE algorithm [20], used by the engineering and architectural communities.
- The Iqbal model [188], which offers extra-accuracy over more conventional models.

Several approaches are now being developed based on NDFD created by different countries. In [291] a preliminary evaluation of a simple solar radiation forecast model using sky cover predictions from the NDFD of the USA as an input. The models developed by [165–168] provide predictions of clear-sky direct and diffuse broadband irradiance with great accuracy when detailed and accurate input data are available.

2.4.2 Decomposition Models

Development of correlation models that predict the beam or sky radiation using other solar radiation measurements is possible [399]. Decomposition models normally use information only on global irradiance to predict the beam and sky components. These relationships are usually expressed in terms of the irradiation which are the time integrals (usually over 1 h) of the radiant flux or irradiance. Examples of different decomposition models developed to estimate direct and diffuse irradiance from global irradiance can be found in [6, 399] and cited references.

2.4.2.1 An Example of a Model of the Solar Irradiance

Solar radiation undergoes changes due to its daily cycle and to passing clouds. In this subsection, the approximation given by [101] has been adopted to obtain a clear-day prediction of the solar irradiance.

The magnitude of the solar radiation at a determined point on the Earth's surface varies mainly with the geographical localization and the day of the year and also with the meteorological characteristics of the chosen instant. To calculate the global irradiance level on a surface, the extraterrestrial irradiance level E_c (solar constant¹) must be known. This value reaches the atmosphere of the Earth with a small modification E_{ext} , due to the elliptical trajectory of the Earth around the Sun.

As the radiation heats the atmosphere, fragmentation is produced, one part is reflected outside and another part is absorbed by the atmosphere; the rest penetrates the atmosphere. One part of this is dispersed, the other is reflected and the rest reaches the Earth in the form of direct irradiance E_b .

¹This is the amount of total energy that contains the extraterrestrial solar irradiance, integrated in all the spectrum of wave lengths. The value used is $E_c = 1367 \text{ W/m}^2$.

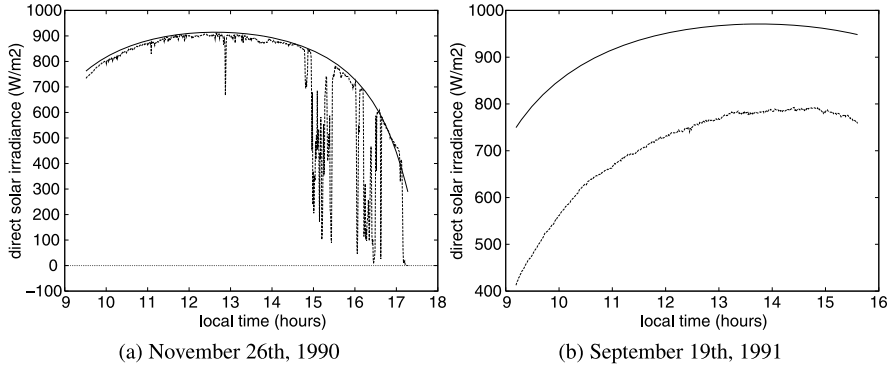


Fig. 2.3 Direct solar irradiance and clear-day prediction

Part of the amount of irradiance reflected and dispersed reaches the Earth in the form of diffuse irradiance. The irradiance that reaches the atmosphere is the solar constant multiplied by the eccentricity correction factor e_{xc} :

$$E_{ext} = E_c \left(\frac{D_0}{D} \right)^2 = E_c e_{xc}; \quad e_{xc} = 1 + 0.033 \cos \left(\frac{2\pi J}{365} \right) \quad (2.21)$$

D being the Sun–Earth distance at a determined instance and D_0 its mean value and J is the Julian Day.

An approximation to the instantaneous value of direct solar irradiance is the one obtained by [101]:

$$E_b = 0.9751 E_{ext} T_b \quad (2.22)$$

where T_b is the transmittance of the direct normal irradiance, which depends on factors such as the ozone cover thickness, the thickness of the water steam cover, two coefficients of atmospheric cloudiness and the air mass at standard pressure.

Expression (2.22) has been used to predict the evolution of the solar irradiance and then compared to the actual direct solar irradiance measured at the PSA. Figure 2.3(a) corresponds to a day with high solar radiation levels in which, at the end of the daily operation, large clouds appeared, while Fig. 2.3(b) corresponds to a day with low solar radiation levels, due to the presence of contamination in the air, but without the presence of passing clouds. As can be seen, lines have been drawn depending on the local hour. By using the prediction model, a filtered value of the solar radiation evolution is directly obtained.

2.4.3 Statistical Models

The perturbation variables are usually represented as time-series structures due mainly to their stochastic behavior. Using time-series models is one of the ways to estimate future values of disturbances. These models are obtained using past data

and are used to estimate the future behavior along a prediction horizon [311]. Time-series models are based on the assumption that the modeled data are autocorrelated and characterized by trends and seasonal variations. Thus, well-known autocorrelated models (ARMA, ARIMA, ARMAX, ARIMAX) could be also used for disturbance estimation [261, 311, 410]. On the other hand, ANN provides also a good solution to perform estimations because its design is based on training and no statistical assumptions are needed for the source data. Neural networks are widely accepted as a technology to predict time-series offering an alternative way to solve complex problems [283, 409]. In [311] a comparison between several types of time-series model was performed: regression models, unobserved component models (UCM), ARIMA models, transfer function models, neural networks and hybrid models (combining regressions and neural nets). In [132] a total of 18 empirical models in linear, quadratic, cubic, logarithmic, exponential and hybrid forms using only sunshine hours, latitude and altitude were compared to estimate monthly average daily global solar radiation on a horizontal surface for 159 weather stations in Turkey.

In this section, a summary of the results in [288] is included, where four different well-known time-series methods are analyzed and compared, namely, Discrete Kalman Filter [337], Discrete Kalman Filter with Data Fusion [279], Exponentially Weighted Moving Average [381] and Double Exponential Smoothing [268]. These methods are used to obtain forecasts of the direct solar irradiance using real data. The nomenclature that will be used in next sections is the following: $z(k)$ is the measurement in the discrete-time instant k and $\hat{x}(k+1)$ is the predicted value one sample ahead.

2.4.3.1 Discrete Kalman Filter

The Kalman Filter (KF) addresses the general problem of trying to estimate the state $x \in \mathbb{R}^n$ of a discrete-time process that is governed by a linear stochastic difference equation. Matrix \mathbf{A} in the difference equation, Eq. (2.23), relates the state at the previous time step $k-1$ to the state at the current step k and matrix \mathbf{H} in (2.24) relates the state to the measurement value $z(k) \in \mathbb{R}^n$ [337].

$$x(k) = \mathbf{A}x(k-1) + w(k-1) \quad (2.23)$$

$$z(k) = \mathbf{H}x(k) + v(k) \quad (2.24)$$

The random variables $w(k)$ and $v(k)$ represent the process and measurement noise, respectively. They are assumed to be independent (of each other), white and with normal probability distributions. The KF estimates a process by using a form of feedback control: the filter estimates the process state at some time and then obtains feedback in the form of noisy measurements. As such, the equations for the KF fall into two groups: time update equations and measurement update equations. The discrete KF time update equations are [337]

$$\hat{x}(k)^- = \mathbf{A}\hat{x}(k-1) \quad (2.25)$$

$$\mathbf{P}(k)^- = \mathbf{A}\mathbf{P}(k-1)\mathbf{A}^T + \mathbf{Q} \quad (2.26)$$

and the discrete KF measurement update equations:

$$\mathbf{K}(k) = \mathbf{P}(k)^- \mathbf{H}^T (\mathbf{H} \mathbf{P}(k)^- \mathbf{H}^T + \mathbf{R})^{-1} \quad (2.27)$$

$$\hat{\mathbf{x}}(k+1) = \hat{\mathbf{x}}(k)^- + \mathbf{K}(k)(z(k) - \mathbf{H}\hat{\mathbf{x}}(k)^-) \quad (2.28)$$

$$\mathbf{P}(k) = (\mathbf{I} - \mathbf{K}(k)\mathbf{H})\mathbf{P}(k)^- \quad (2.29)$$

where $\mathbf{P}(k)^-$ is the a priori estimate error covariance, $\mathbf{P}(k)$ is the a posteriori estimate error covariance, $\hat{\mathbf{x}}(k)^-$ is the a priori estimate, and \mathbf{I} is the identity matrix of the appropriate size. In practice, the process noise covariance \mathbf{Q} and measurement noise covariance \mathbf{R} matrices might change with each time step or measurement, however here we assume they are constant. Detailed information about KF implementation can be found in [396].

2.4.3.2 Discrete Kalman Filter with Data Fusion

The main structure of the discrete Kalman Filter with Data Fusion (KFDF) has the same formulation as in the previous section, with the exception that data fusion is performed. Assume now that we are dealing with two different measurements that provide a reading for some variable of interest z . We call z_1 the measure from the first source and z_2 the measure from the second source. If both measurements are equally good (the quadratic standard deviation $\sigma_1^2 = \sigma_2^2$), we just take the average of both numbers. In this case, a weighted average of both measurements can be obtained to generate an estimation of z , $\hat{\mathbf{x}}(k+1)$. One possibility is weighting each measurement inversely proportional to its precision, that is [279],

$$\hat{\mathbf{x}}(k+1) = \frac{z_1(k)\sigma_2^2 + z_2(k)\sigma_1^2}{\sigma_1^2 + \sigma_2^2} \quad (2.30)$$

Note that the above estimation can be also rewritten as

$$\hat{\mathbf{x}}(k+1) = z_1(k) + K(z_2(k) - z_1(k)) \quad (2.31)$$

where now $K = \sigma_1^2/(\sigma_1^2 + \sigma_2^2)$. The update equation has the same general form as in the previous paragraph (see [279] for further information). In what follows, the measurement z_1 is a real value from a sensor and z_2 is an estimated value calculated using a theoretical model [288].

2.4.3.3 Exponentially Weighted Moving Average

Exponentially Weighted Moving Average (EWMA) is commonly used with time-series data to smooth short-term fluctuations and highlight longer-term trends or cycles. The threshold between short and long terms depends on the application and the parameters of the moving average will be accordingly set. Mathematically, a moving average is a type of convolution and so it is also similar to a low-pass filter used in signal processing [68]. The arithmetic assumption of moving average assumes

that only the latest values have an effect on the current value. However, the moving average assigns equal weight to each value as compared to the trend line that gives weight to only the first and the last values for determination. The long-term moving averages can be useful for measuring the trend whereas the short-term averages can be utilized for measuring the changes in the trend [63, 381]:

$$\hat{x}(k+1) = \frac{z(k) + (1 - \beta_s)z(k-1) + \cdots + (1 - \beta_s)^N z(k-N)}{1 + (1 - \beta_s) + \cdots + (1 - \beta_s)^N} \quad (2.32)$$

where N is the sample window size and $\beta_s \in (0, 1)$ is the smoothing parameter. The sample window is composed by the N most actual samples of analyzed variable from $z(k)$ to $z(k-N)$. When the prediction for time instant $k+1$ is done, its value is located at first place in a sample window which is organized as $[\hat{x}(k+1), z(k), z(k-1), \dots, z(k-N+1)]$. This sample window is used to make the prediction of value in time instant $k+2$ and so on. When the process reaches the prediction horizon, a new sample window is formed from the last N measurements.

2.4.3.4 Double Exponential Smoothing

The Double Exponential Smoothing (DES) is described by the following equations [268]:

$$\chi(k) = \alpha_D z(k) + (1 - \alpha_D)(\chi(k-1) + b_D(k-1)) \quad (2.33)$$

$$b_D(k) = \gamma_D(\chi(k) - \chi(k-1)) + (1 - \gamma_D)b_D(k-1) \quad (2.34)$$

where $\chi(k)$ is the unadjusted forecast, $b_D(k)$ is the estimated trend, α_D is the smoothing parameter for data and γ_D is the smoothing parameter for trend. Note that the current value of the series is used to calculate its smoothed value replacement in double exponential smoothing. The one-period and m -periods ahead forecasts are given, respectively, by

$$\hat{x}(k+1) = \chi(k) + b_D(k) \quad (2.35)$$

$$\hat{x}(k+m) = \chi(k) + mb_D(k) \quad (2.36)$$

There are a variety of schemes to set initial values for χ and b_D in double smoothing, but in [288] $\chi(1) = z(1)$ and $b_D(1) = (z(1) + z(2) + z(3))/3$ as suggested in [268]. The first smoothing equation adjusts χ directly for the trend of the previous period, $b_D(k-1)$, by adding it to the last smoothed value, $\chi(k-1)$. This helps to eliminate the lag and brings χ to the appropriated base of the current value. Then, the second smoothing equation updates the trend, which is expressed as the difference between the last two values. The equation is similar to the basic form of single smoothing, but here it is applied to the updating of the trend. The values for α_D and $\gamma_D \in (0, 1)$ can be obtained via optimization techniques as described in [268].

Table 2.2 Performance indices (courtesy of A. Pawlowski et al., [288])

MSE	RMSE	nRMSE	R^2
$\frac{1}{N} \sum_{k=1}^N (\hat{x}(k) - z(k))^2$	$\sqrt{\frac{1}{N} \sum_{k=1}^N (\hat{x}(k) - z(k))^2}$	$\frac{\sqrt{\frac{1}{N} \sum_{k=1}^N (\hat{x}(k) - z(k))^2}}{\sqrt{\frac{1}{N} \sum_{k=1}^N (z(k))^2}}$	$\frac{\sum_{k=1}^N (\hat{x}(k) - \bar{z})^2}{\sum_{k=1}^N (z(k) - \bar{z})^2}$

2.4.3.5 Illustrative Results

The predicted results for each combination were compared statistically using four different parameters [283]: the Mean Square Error (MSE), the Root Mean Square Error (RMSE), the normalized RMSE (nRMSE), and the Coefficient of Determination R^2 (Table 2.2). When a zero value is obtained for MSE, it means that the estimator $\hat{x}(k)$ predicts observations of the parameter $z(k)$ with perfect accuracy. The unbiased model with the smallest MSE is generally interpreted as the one best explaining the variability in the observations. RMSE is a frequently used measurement of the differences between root mean square error values predicted by a model (or an estimator) and the values actually observed from the variable being modeled or estimated. The nRMSE measurement is useful for comparison while R^2 is used in the context of statistical models, where its main purpose is the prediction of future outcomes on the basis of other related information (it is the proportion of variability in a data set that is accounted for by the statistical model). It provides a measurement of how well future outcomes are likely to be predicted by the forecast method.

Additionally, two measurements of the error are used to show the quantitative variation of the forecasts. These measurements are the average absolute error \bar{e} and the average percent error $\bar{e}_\%$:

$$\bar{e} = \frac{1}{N} \sum_{k=1}^N |z(k) - \hat{x}(k)|, \quad \bar{e}_\% = \frac{1}{N} \sum_{k=1}^N \frac{|z(k) - \hat{x}(k)|}{|z(k)|} 100\% \quad (2.37)$$

The meteorological data used in this section have been recollected during one year by a meteorological station located at the Almería, Spain, 36°46'N2°48'W. For this database, solar irradiance samples are acquired every minute. As commented above, the KFDF technique requires a theoretical model to obtain data for fusion purposes. In this case, the model for direct irradiance explained in Sect. 2.4.2.1 has been used [42, 85].

All the presented methods have some parameters to be set and which have a great influence on the overall performance and accuracy of the forecast. Therefore, a calibration stage with 10 days was performed in order to set up the appropriated values for these parameters, where the minimization of the RMSE error was selected as a reference measurement. The selected days for this calibration process include diverse situations of the solar radiation from different year seasons.

Figures 2.4 and 2.5 present the results for a day with clouds alteration for two prediction horizons of 5 and 15 samples, respectively. The original solar irradiance time-series is characterized by many local changes of trend caused by passing clouds. For the 5-sample horizon, the DES, KF and EWMA methods produce a

Fig. 2.4 Day with passing clouds and a 5-sample horizon (courtesy of A. Pawlowski et al., [288])

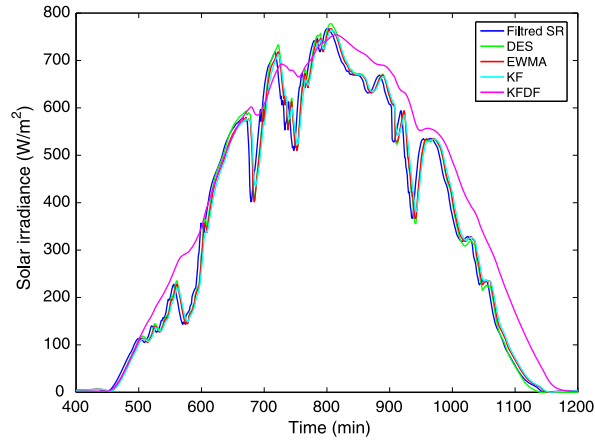
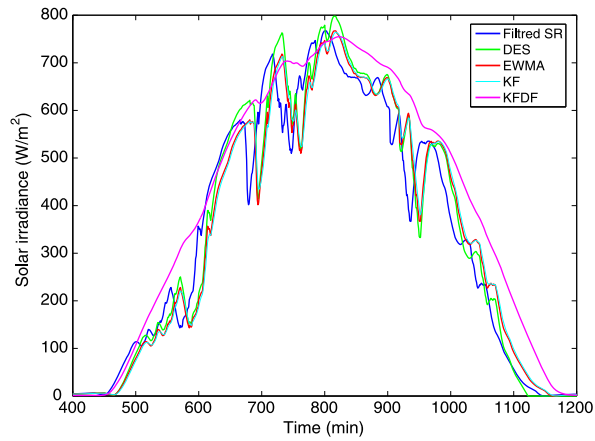


Fig. 2.5 Day with passing clouds and a 15-sample horizon (courtesy of A. Pawlowski et al., [288])



small predicted signal delay. The KFDF technique keeps the theoretical data trend despite of changes in real signal and produces only a slow decrease of the forecasted value. Comparing Figs. 2.4 and 2.5, it can be observed that the signals are characterized by a delay, which is more visible for the last case. In comparison with the rest of the methods, the DES technique produces forecasts that slightly surpass the magnitude of real solar irradiance signal.

Table 2.3 compares the performance indices for the day with passing clouds. The RMSE and nRMSE measurements indicate that the best results for all techniques are generated by the DES method. The second one according to this measurement is the EWMA method. The R^2 for the maximal horizon reaches the highest value 0.9848 for the DES method. However, the worst value is obtained by the KFDF. Furthermore, for this analysis, the lowest value of the average absolute error \bar{e} for 15-sample horizon is obtained for the DES technique with a value of 26.22 W/m². The outcome of average percentage error $\bar{e}_{\%}$ is 32% for the DES method and for the

Table 2.3 Performance comparison for a day with passing clouds (courtesy of A. Pawlowski et al., [288])

Index	Horizon	KF	KFDF	EWMA	DES
MSE	5	676.7	2966	470.5	461.8
	10	1563	3700	1323	1280
	15	2508	4296	2260	2167
RMSE	5	26.01	54.46	21.69	21.49
	10	39.54	60.83	36.38	35.78
	15	50.08	65.54	47.54	46.55
nRMSE	5	0.080	0.168	0.067	0.066
	10	0.122	0.188	0.112	0.110
	15	0.155	0.202	0.147	0.144
R^2	5	0.9949	0.9858	0.9965	0.9966
	10	0.9883	0.9827	0.9901	0.9909
	15	0.9812	0.9805	0.9831	0.9848
\bar{e} [W/m ²]	5	13.86	31.43	11.09	10.70
	10	21.90	35.31	19.59	18.59
	15	28.56	38.37	26.45	24.69
$\bar{e}_{\%}$ [%]	5	14.89	77.37	10.89	17.21
	10	26.07	89.55	22.12	26.22
	15	37.18	100.76	33.42	32.37

EWMA and KF it is 33% and 37%, respectively. The KFDF technique produces an unacceptable percentage error for the 15-sample horizon.

2.4.3.6 Computational Intelligence-Based Models

Several methods for forecasting solar irradiance in different time scales have appeared recently [250] based on ANN, fuzzy logic and hybrid system such as AN-FIS, ANN-wavelet and ANN-genetic algorithms (GA). These approaches can be classified into three different types [249, 250].

- The first one can estimate the solar irradiance (in different scale times) based on some meteorological parameters such as air temperature, relative humidity, wind speed, wind direction, cloud, sunshine duration, clearness index, pressure and geographical coordinates as latitude and longitude. Multilayer Perceptron (MLP) network, Radial Basis Function (RBF) network and fuzzy logic can resolve this problem [249, 250].
- A second approach allows predicting the future solar irradiance (in different scale times) based on the past observed data [250]. Therefore, in this case recurrent

neural networks (RNN), wavelet-networks and wavelet-networks-fuzzy are very suitable.

- The last one combines the two previous approaches, so that different ANN-architectures and ANFIS are adequate.

Other examples of these approaches can be found in [250] and the cited references. Representative cases can be found in [409], where the thermal energy collection of solar heat energy utilization system based on solar radiation forecasting at one-day ahead 24-hours thermal energy collection is performed using three different ANN models trained by weather data based on tree-based model and tested according to forecast day. Selected models are feedforward neural network (FFNN), radial basis function neural network (RBFNN) and RNN. In [250] a practical method for solar irradiance forecast using ANN is presented. The proposed MLP model makes it possible to forecast the solar irradiance on a base of 24 h using the present values of the mean daily solar irradiance and air temperature. In [123] ANN are applied to multi-step long-term solar radiation prediction. The networks are trained as one-step-ahead predictors and iterated over time to obtain multi-step longer-term predictions. Auto-regressive solar radiation models and solar radiation models auto-regressive with exogenous inputs are compared, considering cloudiness indices as inputs in the latter case. These indices are obtained through pixel classification of ground-to-sky images. The input-output structure of the ANN models is selected using evolutionary computation methods.

As pointed out by [311], several problems with ANN have been noted in the literature, related with the existence of local minima, noise over-fitting and others. The problems with neural nets have been one motivating factor in the development of new classes of model combining nets with other techniques. One idea is to combine ANN with wavelets [91, 92], and regressions and ANN [180, 421]. Typically, in these hybrid models, an initial regression or ARIMA is estimated and the residuals are then processed using a neural net. The forecasts from the two separate stages are then combined.

2.5 Control of the Energy Conversion Units

As pointed out in the introduction of the chapter, the control of the variables associated to the solar conversion units depends very much on the type of system. In the case of photovoltaic (PV) systems, this involves the control of the voltage and intensity produced by the solar cells in order to operate at the maximum efficiency point and the control of the associated DC/AC conversion power electronics.

In the case of thermal solar plants, a HTF is heated and thus associated temperatures and flows have to be controlled, as well as temperature, flow, and pressure of the produced steam. Values of solar irradiance are used to compensate for its variations. Once the steam is produced, the controls at this level do not differ much from the control of other thermal plants. In most cases oil is used as energy conversion fluid and because oils decompose and generate dangerous inflammable fumes at relative low temperatures, the maximum operating temperatures have to be kept below

these temperatures, which are rather low. In order to increase the performance of the steam generating units, the solar field has to be operated close to the maximum operating temperatures.

The control of energy conversion units will be treated in detail in the following chapters.

2.6 Integrated Control

Solar energy is intermittent and is not always available when needed and where needed. Because of that, the integration of solar energy plants in the electrical grid is a challenging problem. Energy storage is a potential solution to the integration problems. An efficient operation of solar plants with energy storage systems could allow a closer match between solar plants power generation and electrical power demand. In thermal solar power plants, energy is usually stored as heat. Heat storage systems allow solar thermal plants to produce electricity at night and on cloudy days. Additionally, the equipment (steam generators turbines and electrical generator) does not need to be designed for the peak power but for the average power and thus installation costs are reduced. Furthermore, equipment can operate continuously with smaller payback periods. When collected solar power is higher than the demanded energy, excess heat is transferred to a thermal storage medium and stored in an insulated reservoir. The stored heat can be withdrawn for power generation when needed. Different systems have been used in solar power plants such as molten salts, pressurized steam, change materials and concrete. Energy storage tanks are usually well insulated and can store energy for a few days and provide enough thermal storage for a few plant operational hours.

The price of electricity is determined by a variety of methods which change not only from place to place, but also with the commissioning date of the plants. Furthermore, proposals of new price mechanisms are appearing continuously with the liberalization of the energy prices and they are considered to be a fundamental part of the Smart Grid concept. In the electrical energy market, the price fluctuations will tend, usually, to correlate well with the hourly demand because the prices will try to cover the marginal cost of generation which will normally increase with demand. Risk factors are also considered for establishing prices, for example, the available generators to cope with unexpected demand peaks will affect the electricity price.

The use of renewable energies is encouraged in many countries by different policies such as FIT which guarantees grid access and long-term contracts for the electricity produced by renewable sources at the cost of renewable energy generation and which tends toward market prices with time. The electrical utilities or regional or national authorities are obliged to buy the renewable electricity from the renewable energy producer. The FIT are determined to make it possible for an installation to be operated cost-effectively if the installation is managed efficiently and state of the art techniques are used. FIT may therefore differ depending on the sources, location, project size and other important factors.

Solar plant operators can benefit from energy storage systems by shifting generation from valley periods to peak periods taking advantage of the corresponding price variations. Two different scenarios will be analyzed in Chap. 8: (a) non-committed production, where the electrical utilities buy all the production of the solar power plant at prices at fixed prices and, (b) committed production, where the solar plant and the utility agree to a production and price in advance. The electrical utility penalizes the deviation with the agree contract.

If the prices are constant, the best option would be to produce as much electrical energy as possible. Storage can be used in those situations where more solar energy can be collected than energy converted and delivered. This may be due to maintenance operation or turbines or generator having been designed for nominal conditions below the maximum solar conditions.

If prices vary with the time of day or if the production is committed with penalization errors, the energy storage can be used to maximize profits. The electrical energy produced depends basically on the solar radiation during that sampling period and on the operating conditions of the plant. For example, when the plant is starting up, some of the solar energy will need to be used to warm up the plant systems to the operative stage while if the plant was already generating electricity in the previous period, no energy will be needed for warming up. Furthermore, the warming up of the plant will require some time.

The electricity market works with different models. In many of them, the hourly daily price is fixed by a negotiation procedure. First, usually in the morning, a period opens for filing buying and selling offers for the energy for every hour of the day. There are two types of decision that have to be taken. First, at the beginning of the day, to determine the offer for the next 24 hours and once this have been agreed, the next problem is to determine, for each time period, the power to be delivered and the power to be stored in order to maximize profits and fulfill all operational objectives. Since solar energy cannot be exactly predicted in advance, the optimization problems involved have to be formulated in an uncertain framework. The performance of solar plants depends on the environmental and plant operating conditions. Plant operation conditions (modes and set points of fundamental variables) have to be determined by the control system in order optimize plant performance.

All these issues will be discussed in Chap. 8.

2.7 Summary

This chapter has been devoted to describing the control problems found in solar energy systems. Four different levels can be distinguished: (i) the control of the solar collector units, (ii) solar radiation estimation and forecast, (iii) the control of the energy conversion systems and (iv) the overall control of the complete process. In the case of the control of the solar collector units and solar radiation estimation and forecast, an overview of the fundamentals and techniques has been carried out, including some illustrative results. The next chapter will deal with the modeling and control of the energy conversion systems and the overall control of the complete process.

Control of Solar Energy Systems

Camacho, E.F.; Berenguel Soria, M.; Rubio, F.R.;
Martínez, D.

2012, XXXIV, 418 p., Hardcover

ISBN: 978-0-85729-915-4